Preprint version

Development and Experimental Validation of a Reconfigurable Free-Floating Space Manipulator Testbed for In-Space Servicing

Daegyun Choi*, Diego Quevedo†, Rajat Chadha‡, and Donghoon Kim§
Department of Aerospace Engineering & Engineering Mechanics
University of Cincinnati
Cincinnati, OH, USA
Email: *Daegyun.Choi@uc.edu, †queveddo@mail.uc.edu, ‡rajatrt@mail.uc.edu, §Donghoon.Kim@uc.edu

***Abstract*—As space missions grow in complexity, the importance of in-space servicing, assembly, and manufacturing is increasing. Space manipulator systems are essential for these operations, yet the dynamic coupling effects in free-floating environments can hinder the system's stability. This work presents the construction and experimental validation of a reconfigurable dual-arm-mounted free-floating spacecraft testbed. Unlike existing testbeds with fixed parameters, the proposed system allows for systematic adjustment of link lengths and mass properties to study their influence on the dynamic coupling. Experimental results demonstrate reliable tracking performance of joint controllers. Furthermore, the implementation of reaction-minimized manipulation successfully reduces the base's reactive motion by approximately five times compared to standard operation. This work establishes a multi-purpose on-ground testbed for verifying diverse in-space servicing mission scenarios.**

***Index Terms*—space manipulator systems, reconfigurable robotic manipulators, dynamic coupling, air-bearing testbed**

I. Introduction

Since the beginning of the space age, the number of spacecraft launched into orbit has escalated exponentially, particularly with the recent emergence of mega-constellations in low Earth orbit [1]. Historically, space missions were dominated by expendable approaches in which assets were decommissioned upon reaching the end of their lifespans, fuel depletion, or component failure [2]. However, growing concerns regarding space debris and the prohibitive costs of launches have necessitated a shift toward sustainable orbital operations. In this context, In-space Servicing, Assembly, and Manufacturing (ISAM) has emerged as an innovative solution, enabling repair, refueling, assembly of large structures, and part replacement in orbit [3].

Successful ISAM missions demand high autonomy and precise control [4]. Key technical requirements include Rendezvous, Proximity Operations, and Docking (RPOD) for safely accessing resident space objects, and robotic manipulator control capable of performing precise tasks while mitigating contact impacts.

Because the space environment is characterized by microgravity and vacuum, developed algorithms and hardware must undergo thorough ground verification before orbital deployment [5]. Various Hardware-In-the-Loop (HIL) simulators and ground test facilities have been developed for this purpose. A review of the existing literature reveals that testbeds for RPOD technology verification have primarily focused on emulating relative motion among multiple satellites. These facilities are broadly classified into two types.

The first category consists of six-Degrees-Of-Freedom (6-DOF) spacecraft simulators. These systems typically combine planar air bearings on granite or epoxy floors with spherical air bearings for rotational motion and vertical kinematic stages for out-of-plane motion replication. Notable examples include the Multi-Spacecraft Testbed for Autonomy Research (M-STAR) [6] at the California Institute of Technology and the ADvanced Autonomous MUltiple Spacecraft (ADAMUS) [7] at Embry-Riddle Aeronautical University.

The second category utilizes robotic manipulators. The European Proximity Operations Simulator (EPOS) [8] at the German Aerospace Center (DLR) combines rail systems and high-precision industrial robotic arms to simulate geometry and sensor data from a long-distance approach to final docking. Another notable example is the DYNamic Attitude-orbital MOtion Simulator (DYNAMOS) [9] at the University of Cincinnati, which integrates a 6-DOF hexapod platform with a 6-DOF robotic arm. This integration establishes a coupled 12-DOF HIL framework designed to achieve precise and dynamic spacecraft motion emulation for executing representative in-space servicing, assembly, and manufacturing mission scenarios.

While these systems effectively verify sensor fusion and docking algorithms, they often face limitations in confirming the complex dynamic coupling effects arising from the interaction between a servicing spacecraft and its robotic manipulator under momentum conservation. In Space Manipulator Systems (SMSs), the movement of a manipulator affects the base spacecraft's position and attitude through dynamic coupling [10]. This phenomenon is a key feature of the microgravity environment governed by conservation of momentum [11]. Air-bearing-based testbeds are suitable for emulating these near-frictionless, momentum-conserving environments in

This material is based upon work supported by the Air Force Office of Scientific Research under award number FA9550-24-1-0600.

a two-dimensional plane. Representative examples include the Spacecraft Proximity Operations Testbed (SPOT) at Carleton University [12] and the POSEIDYN (Proximity Operation of Spacecraft: Experimental hardware-In-the-loop DYNamic) simulator at the Naval Postgraduate School [13].

However, a limitation of many current SMS testbeds is the lack of physical reconfigurability. Most existing robotic platforms utilize manipulators with fixed link lengths and static mass distributions. In actual space missions, manipulators must be optimized based on target geometry or specific mission requirements, which necessitates the verification of various design parameters during the development phase [14]. Focusing on this necessity, this work presents the development and capabilities of an SMS testbed equipped with two reconfigurable robotic manipulators. The system allows for the emulation of various mission profiles and scales by adjusting the link lengths and mass properties of the multi-body systems to maintain dynamic similarity between the ground-based experimental model and the intended flight-model spacecraft.

The key contributions of this study are: i) the development of an air-bearing-based motion testbed equipped with reconfigurable robotic arms emulating free-floating SMS motion on a plane, and ii) the experimental validation of key SMS mission scenarios based on joint trajectory tracking.

II. Testbed Design and Construction

The developed testbed, an upgraded dual-arm version of the previous single-arm system [15], emulates planar free-floating SMS dynamics. It integrates a frictionless air-bearing platform with two reconfigurable 3-DOF robotic arms to study dynamic coupling and autonomous control for in-space servicing. The design satisfies the following core requirements:

- **Free-floating emulation**: Replicates microgravity conditions using a near-frictionless air-bearing system on a precision granite surface.
- **Systematic reconfigurability**: Allows independent adjustment of link length and mass, enabling isolation of design parameters influencing dynamic coupling.
- **Real-time sensing and control**: Features real-time state acquisition (base yaw, joint angles, and joint velocities) and closed-loop feedback control.

A. Air-bearing Platform

The platform operates on a granite table. Four air bearings, supplied by pressurized air, create a thin film for horizontal motion. To optimize dynamic stability, mass is strategically distributed: the heaviest components (air tanks) are installed in the bottom layer to lower the center of mass, while electronics and sensors are positioned in the upper layer [15].

For the upgraded version, the top layer was modified to accommodate a second manipulator. The modified platform, shown in Fig. 1, has a total mass varying between 22.5 and 23.4 kg depending on air levels. For real-time sensing, a BNO055 9-DOF Inertial Measurement Unit (IMU) is integrated to measure the base yaw rate.

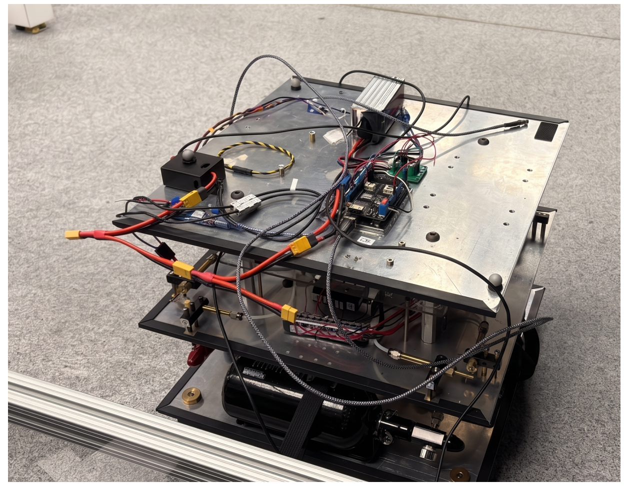

Fig. 1. Air-bearing platform without arms.

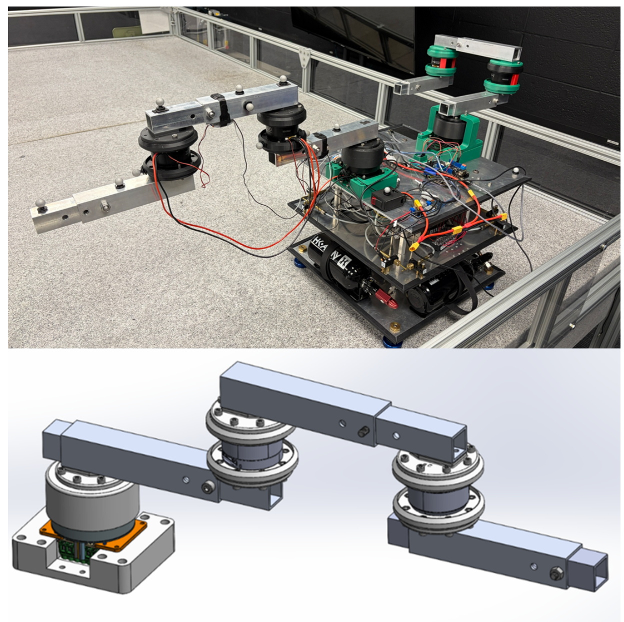

Fig. 2. Reconfigurable SMS platform (top) and reconfigurable 3-DOF manipulator Computer-Aided Design (CAD) model (bottom).

B. Reconfigurable Robotic Arms

The testbed features two custom three-link, 3-DOF revolute joint robotic arms, shown at the top of Fig. 2. The design follows several constraints:

- **Safety:** Total length and motion limits prevent table boundary or self-collisions.
- **Mass & Torque:** High-torque, low-mass motors actuate the joints within the platform's payload capacity.
- **Modularity:** Links allow independent adjustment of length and mass to study their influence on coupling [15].

Each arm link consists of 6063 aluminum base links and extension tubes, shown at the bottom of Fig. 2. Allowable link length variations range between 200 and 400 mm, with a nominal length of 300 mm [15].

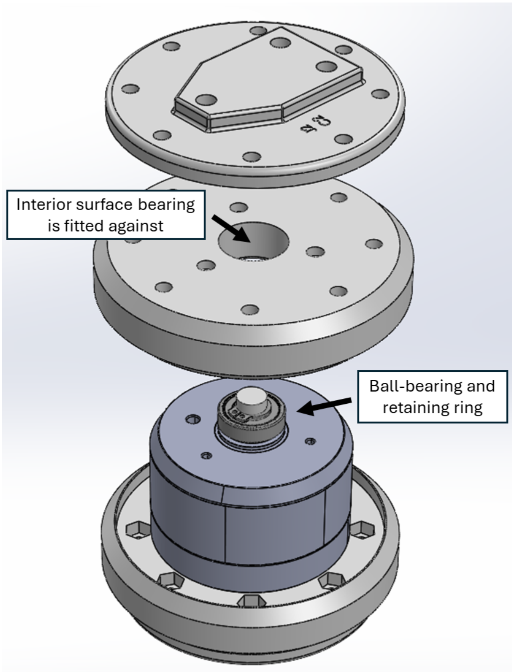

Fig. 3. Joint attachment for Joint 2 and 3.

The payload capacity is conservatively restricted to 1 kg at the maximum reach (link lengths of 400 mm) to prevent excessive static deflection. Such deflection can tilt the vertical joint axes, introducing unmodeled disturbance torques on the joints, violating the planar motion assumption of the testbed.

Joint 1 utilizes a high-torque ODrive M8325s motor, while Joints 2 and 3 use lightweight RoboMaster GM6020 motors to minimize manipulator mass.

In a previous version of the platform developed by the authors' group [15], structural jittering was observed in the second joint due to bending under the distal link weight. As an improvement in the current iteration, this issue was eliminated by utilizing the hollow-center design of the motors in conjunction with improved joint attachments, as illustrated in Fig. 3. A shaft was integrated through the motor center and supported by a ball bearing, which significantly increased the bending stiffness. Although the current testbed includes dual arms for multi-arm research, this study employs a single active arm; the second arm is locked in a stowed configuration and treated as a static component of the base spacecraft inertia.

C. Software Architecture

The software is organized into two layers communicating over a high-speed serial link: i) an embedded firmware layer running on a MicroController Unit (MCU) for real-time motor control and data acquisition, and ii) a host-PC layer in Python for trajectory planning and data recording. This architecture is shown in Fig. 4.

1) Subsystem Communication: Actuator commands and feedback are exchanged over a CAN bus at 1 Mbit/s via an MCP2515 SPI–CAN transceiver. The MCU communicates with

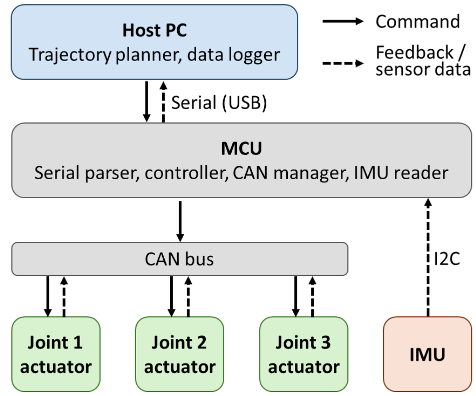

Fig. 4. Embedded control and communication architecture of the developed testbed.

the host PC via a USB (Universal Serial Bus)–UART (Universal Asynchronous Receiver/Transmitter) bridge at 1 Mbit/s. Command signals are streamed from the PC at every 10 ms control tick, while telemetry regarding base and joint states is broadcast by the MCU at 100 Hz.

2) Sensing: Each actuator provides position feedback over the CAN bus. Joint 1 uses ODrive encoder units converted to degrees, while Joints 2 and 3 use 14-bit absolute encoders with firmware-level rotation counters to track multi-turn travel. The base attitude is measured by a BNO055 IMU via I2C at 400 kHz. The firmware reads the gyroscope z-axis at 100 Hz, providing the yaw. The host PC integrates these timestamps to produce the cumulative yaw angle, quantifying the reaction motion induced on the base.

3) Control Command Generation: At each 10 ms time step, the trajectory manager in the host PC reads pre-computed joint angle and velocity profiles and transmits position–velocity pairs to the MCU. The control implementation differs by motor type:

- **Joint 1:** Driven by the ODrive's internal closed-loop controller configured in the velocity mode. The firmware converts target angles and rates into revolution-based units and forwards them as velocity feed-forward commands over the CAN bus.
- **Joints 2 and 3:** Controlled by discrete-time proportional-integral-derivative controllers implemented directly within the MCU firmware. These controllers utilize velocity feed-forward to improve tracking and anti-windup clamping on the integral term to prevent saturation during high-acceleration maneuvers.

The overall specifications of the developed reconfigurable manipulator-equipped testbed are summarized in Table I.

III. Experimental Validation

Experiments were conducted to evaluate the performance of the reconfigurable SMS testbed. Although the platform is designed as a dual-arm system, this validation stage focuses on single-arm maneuvers (with a specific link length and mass) by locking the second arm in a fixed configuration. This

TABLE I
TESTBED SPECIFICATIONS

Parameter	Value
Platform dry mass (excluding arms)	22.5 kg
Robotic arms mass	5.86 kg
Usable gas mass	0.90 kg
Total wet mass	29.26 kg
Estimated operation time	~ 14.5 min
Number of active joints	3 (1-DOF revolute each)
Link length range (each link)	$200 - 400$ mm
Max. total arm reach	$\sim 1,200$ mm
Max. payload @max. reach	1 kg
Joint 1 angle limit	± 90 deg
Joint 2 and 3 angle limit	± 170 deg
Max. joint velocity	25.2 deg/s
Control loop rate	100 Hz
Telemetry rate	100 Hz

approach manages system complexity during initial characterization while treating the stowed arm as a static component of the base inertia.

The primary mission scenarios aim to analyze the dynamic coupling effect, a chronic challenge for free-floating SMSs, and validate control performance in minimizing base reactive motion. When an SMS performs orbital servicing, arm motion induces base reactions governed by the conservation of momentum, leading to unintended attitude and position changes. To quantify these effects, two distinct scenarios were compared:

- **Standard Manipulation**: The arm is controlled to move the End-Effector (EE) to a desired location without considering the reaction applied to the base.
- **Reaction-minimized Manipulation**: The arm reaches a desired position while simultaneously minimizing reaction torques to suppress disturbances to the base states, particularly attitude.

Reaction-minimized strategies enhance fuel efficiency by reducing the duty cycle of active attitude control systems [16] and ensure stable power generation and communication through consistent solar array and antenna pointing [17].

Currently, task-space control is under integration; thus, this study employs reference joint trajectory tracking. A precise simulation environment was first constructed using CAD-derived parameters. Within this simulation, joint-space reference trajectories were generated for both scenarios and then commanded to the joint motor controllers for real-time tracking.

A. Joint Trajectory Generation

The kinematic relationship between the base velocity, $\dot{\mathbf{x}}_b \in \Re^6$, and an n-DOF arm's joint rate, $\dot{\mathbf{q}}_m \in \Re^n$, is given by:

$$\dot{\mathbf{x}}_b = C_{bm}\dot{\mathbf{q}}_m \tag{1}$$

where $C_{bm} \in \Re^{6\times n}$ is the joint-to-base dynamic coupling matrix. The inertial velocity of the EE, $\dot{\mathbf{x}}_e \in \Re^6$, is determined via the generalized Jacobian $J_g \in \Re^{6\times n}$:

$$\dot{\mathbf{x}}_e = J_g(\mathbf{q})\dot{\mathbf{q}}_m \tag{2}$$

To avoid joint limits, a diagonal weighting matrix, $W \in \Re^{n\times n}$, is introduced with elements [18]:

$$w_i = \left\{1 + \kappa\left(\frac{|q_i|}{q_{\text{lim},i}}\right)^{\alpha}\right\}^{-1} \tag{3}$$

where κ and α are positive scalars, q_i is the i-th joint angle, and $q_{\text{lim},i}$ is the i-th joint angle limit. This penalizes motion as joints approach their physical limits.

1) Standard Manipulation: The objective is to minimize EE position error using the damped weighted minimum norm solution [19]:

$$\dot{\mathbf{q}}_{\text{cmd}} = W\left(J_{g,t}\right)^T\left\{J_{g,t}W\left(J_{g,t}\right)^T + \lambda_m^2 I\right\}^{-1}\mathbf{v}_{\text{cmd}} \tag{4}$$

where $\mathbf{v}_{\text{cmd}} = K_p(\mathbf{r}_{\text{des}} - \mathbf{r}_{\text{ee}}) \in \Re^3$ is the commanded EE velocity, $\mathbf{r}_{\text{des}} \in \Re^3$ and $\mathbf{r}_{\text{ee}} \in \Re^3$ are the desired and current EE positions, respectively. Also, $J_{g,t} \in \Re^{3\times n}$ is the translational generalized Jacobian of the manipulator, λ_m is the singularity damping factor, and $K_p \in \Re^{3\times 3}\succ 0$.

2) Reaction-minimized Manipulation: A hierarchical control structure is employed, where base attitude stabilization is the primary task and EE positioning is secondary.

a) Primary Task (Base Attitude Stabilization): The base angular velocity, $\boldsymbol{\omega}_0 \in \Re^3$, is mapped by the joint-to-base rotational dynamic coupling matrix, $C_{bm,r} \in \Re^{3\times n}$:

$$\boldsymbol{\omega}_0 = C_{bm,r}\dot{\mathbf{q}}_m \tag{5}$$

Similar to Eq. (4), the commanded stabilization control is defined as:

$$\dot{\mathbf{q}}_{\text{cmd},1} = W\left(C_{bm,r}\right)^T\left\{C_{bm,r}W\left(C_{bm,r}\right)^T + \lambda_r^2 I\right\}^{-1}\boldsymbol{\omega}_{\text{cmd}} \tag{6}$$

where $\boldsymbol{\omega}_{\text{cmd}} = K_a(\mathbf{0} - \boldsymbol{\theta}_{0/N}) \in \Re^3$ is the command base angular velocity, λ_r is the singular damping factor, and $K_a \in \Re^{3\times 3}\succ 0$.

b) Secondary Task (EE Control): EE control is assigned within the null space of the primary task:

$$\dot{\mathbf{q}}_{\text{cmd},2} = W\left(J_n\right)^T\left\{J_n W\left(J_n\right)^T + \lambda_n^2 I\right\}^{-1}\mathbf{v}_{\text{cmd},2} \tag{7}$$

where $\mathbf{v}_{\text{cmd},2} = (\mathbf{v}_{\text{cmd}} - J_{g,t}\dot{\mathbf{q}}_{\text{cmd},1}) \in \Re^3$, $J_n = J_{g,t}N_r \in \Re^{3\times n}$, λ_n is the singularity damping factor, and $N_r = I - W\left(C_{bm,r}\right)^T\left\{C_{bm,r}W\left(C_{bm,r}\right)^T + \lambda_r^2 I\right\}^{-1}C_{bm,r} \in \Re^{n\times n}$ is the null-space projector. Hence, the total joint rate command of the manipulator is given by $\dot{\mathbf{q}}_{\text{cmd}} = \dot{\mathbf{q}}_{\text{cmd},1} + \dot{\mathbf{q}}_{\text{cmd},2}$.

The simulation parameters for the trajectory generation are listed in Table II.

B. Experiment Results

This section evaluates the operational performance of the reconfigurable testbed. The primary objective is to validate the system's replication of dynamic coupling and confirm its reliability as a research platform. Comparative results are illustrated in Figs. 5–7.

Measured joint angles closely followed reference trajectories in both experiments, validating the reliability of the motor

TABLE II
PARAMETERS FOR JOINT TRAJECTORY GENERATION

Parameter	Value
Simulation time	20 s
Time interval	0.01 s
Desired EE position ($\mathbf{r}_{\text{des}}$)	$[0.55\ 0.25\ 0]^T$ m
Initial joint configuration ($\mathbf{q}_{m,0}$)	$[1\ 1\ 1]^T$ deg
EE position gain (K_p)	$2I_{3\times3}$
Attitude correction gain (K_a)	$15I_{3\times3}$
Penalty coefficient (κ)	10^3
Penalty order (α)	10
Singularity damping factors (λ_m, λ_r, λ_n)	1×10^{-3}
Joint rate limit ($\dot{q}_{\max}$)	30 deg/s
Joint angle limits ($q_{\text{lim},i}$)	$80, 150, 150$ deg

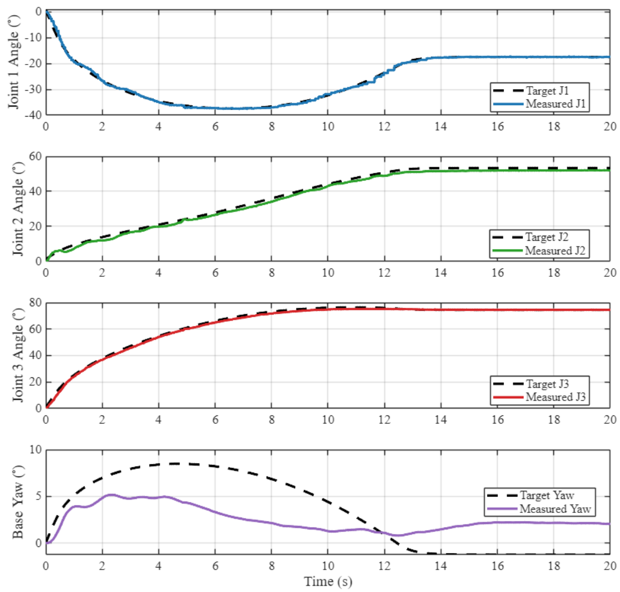

Fig. 5. Joint angles and induced base yaw for standard manipulation.

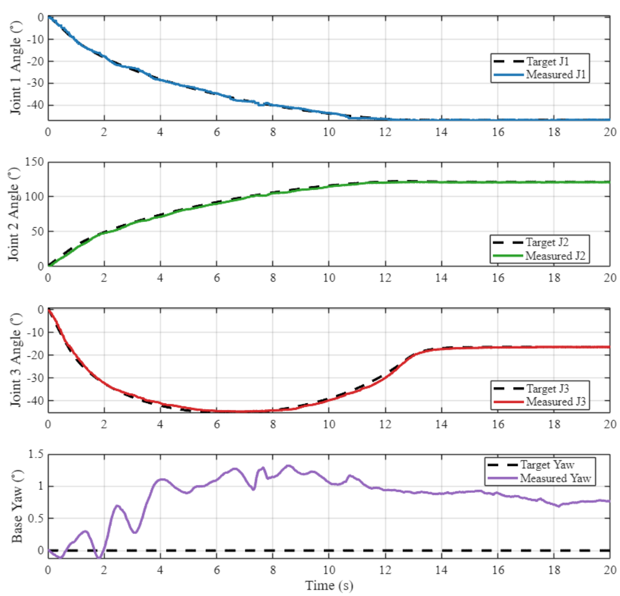

Fig. 6. Joint angles and induced base yaw for reaction-minimized manipulation.

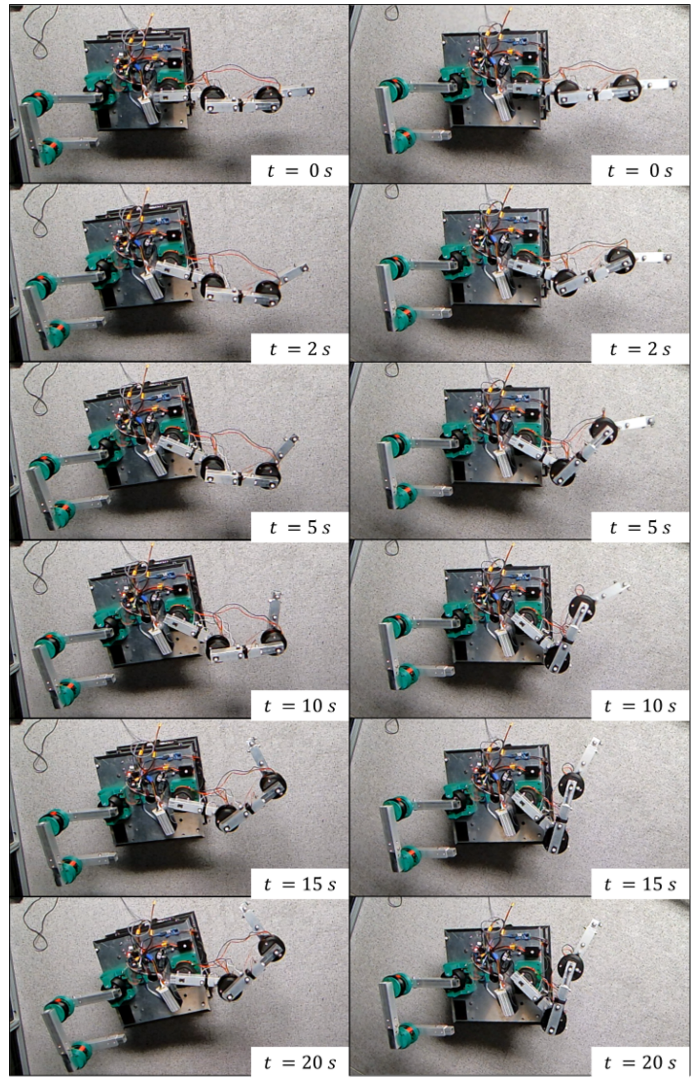

Fig. 7. Experiment time-lapse for the standard manipulation (left) and reaction-minimized manipulation (right).

controllers and ensuring that the base responses were the direct result of intended arm maneuvers.

In the standard manipulation case, minimizing EE position error caused reaction torques to transfer directly to the base, resulting in a hardware-observed yaw disturbance exceeding 5 deg. This typical dynamic coupling phenomenon validates the testbed's ability to emulate the uncompensated motion of a free-floating SMS.

Conversely, under reaction-minimized manipulation, base attitude stabilization was successfully prioritized. The base yaw angle was maintained within a maximum deviation of approximately 1.2 deg, representing a 4-fold reduction in reactive motion compared to standard operation. These results confirm that the null-space projection mechanism effectively redistributes joint velocities to suppress disturbances while achieving the desired EE position. The residual steady-state offsets of approximately 0.8 deg and deviations from simulation are attributed to model-reality mismatch between CAD-derived nominal parameters and physical hardware, highlighting the importance of precise parameter identification in ground-based validation.

Overall, these experiments verify that the testbed successfully captures the dynamic behaviors of an SMS and serves as a valid tool for verifying various mission scenarios through its reconfigurable links and mass properties.

IV. Conclusion

A reconfigurable dual-arm-mounted air-bearing testbed was developed to emulate the dynamic coupling of free-floating orbital systems. Structural jittering identified in a previous version was successfully eliminated through an improved joint design. Experimental validation demonstrated high trajectory tracking precision and a 4-fold reduction in base disturbance during reaction-minimized maneuvers. These results prove the testbed's viability as a research platform. Future work will focus on simultaneous dual-arm operations and the integration of a high-precision external sensing system for task-space control.

References

[1] ESA Space Debris Office, "Esa's annual space environment report," European Space Agency, Tech. Rep. 10, May 2026.

[2] J. Mulvaney, D. Arney, C. Williams, J. Morel, C. Stockdale, C. Whitlock, and V. Balaji, "In-space servicing, assembly, and manufacturing (isam) state of play," NASA, Tech. Rep., 2025. [Online]. Available: https://ntrs.nasa.gov/citations/20250008988

[3] N. Science and T. Council, "In-space servicing, assembly, and manufacturing national strategy," Executive Office of the President of the United States, Tech. Rep., April 2022.

[4] K. Stewart, S. Chapin, R. Leontie, and C. G. Henshaw, "Crossing the sim2real gap between simulation and ground testing to space deployment of autonomous free-flyer control," in *2025 International Conference on Space Robotics (iSpaRo)*, 2025, pp. 524–530.

[5] A. Chhabra and D. Kim, "Ground robotic platform for simulation of on-orbit servicing missions," *Journal of Aerospace Information Systems*, vol. 19, no. 7, pp. 480–493, 2022.

[6] Y. K. Nakka, R. C. Foust, E. S. Lupu, D. B. Elliott, I. S. Crowell, S.-J. Chung, and F. Y. Hadaegh, "A six degree-of-freedom spacecraft dynamics simulator for formation control research," in *AIAA Spaceflight Mechanics Meeting, Galveston TX*, 2018.

[7] D. Gallardo, R. Bevilacqua, and R. Rasmussen, "Advances on a 6 degrees of freedom testbed for autonomous satellites operations," in *AIAA Guidance, Navigation, and Control Conference*, 2011, p. 6591.

[8] H. Benninghoff, F. Rems, E.-A. Risse, and C. Mietner, "European proximity operations simulator 2.0 (epos)-a robotic-based rendezvous and docking simulator," *Journal of large-scale research facilities JLSRF*, 2017.

[9] A. Chhabra and D. Kim, "Dynamos: Design, implementation, and validation of a hardware-in-the-loop simulation testbed for in-space servicing," *IEEE Aerospace and Electronic Systems Magazine*, vol. 41, no. 5, pp. 40–53, 2026.

[10] Y. Xu, "The measure of dynamic coupling of space robot systems," in *Proceedings IEEE International Conference on Robotics and Automation*. IEEE, 1993, pp. 615–620.

[11] G. Das, D. Choi, and D. Kim, "Understanding and utilizing dynamic coupling in free-floating space manipulators for on-orbit servicing," in *2025 AAS/AIAA Astrodynamics Specialist Conference*, 2025.

[12] A. Crain, K. Hovell, C. Savytska, and S. Ulrich, "Optimal capture of spinning spacecraft via deep learning vision and guidance," *Journal of Spacecraft and Rockets*, vol. 62, no. 5, pp. 1727–1739, 2025.

[13] J. Virgili-Llop, J. V. Drew, R. Zappulla, and M. Romano, "Laboratory experiments of resident space object capture by a spacecraft–manipulator system," *Aerospace Science and Technology*, vol. 71, pp. 530–545, 2017.

[14] G. Chen, Z. Huang, Y. Yan, X. An, Z. Zhao, J. Lin, X. Zhao, X. Gao, J. Zong, X. Jia, Z. Yao, J. Liao, and N. Ji, "Key technical fields and future outlooks of space manipulators: A survey," *SmartBot*, p. e70027, 2026.

[15] A. Chhabra, G. Das, D. Quevedo, D. Choi, and D. Kim, "Development of a reconfigurable space manipulator testbed for dynamic coupling analysis," in *2025 IEEE National Aerospace and Electronics Conference (NAECON)*, 2025.

[16] M. A. Torres and S. Dubowsky, "Minimizing spacecraft attitude disturbances in space manipulator systems," *Journal of Guidance, Control, and Dynamics*, vol. 15, no. 4, pp. 1010–1017, 1992.

[17] E. G. Papadopoulos, "Nonholonomic behavior in free-floating space manipulators and its utilization," in *Nonholonomic Motion Planning*. Springer, 1993, pp. 423–445.

[18] T. Chan and R. Dubey, "A weighted least-norm solution based scheme for avoiding joint limits for redundant manipulators," in *Proceedings IEEE International Conference on Robotics and Automation*, vol. 3, 1993, pp. 395–402.

[19] D. N. Nenchev, "Redundancy resolution through local optimization: A review," *Journal of Robotic Systems*, vol. 6, no. 6, pp. 769–798, 1989.